and Electron Transfer Processes; Interscience: New York, 1968.
(7) Gallot, Y.; Rempp, P.; Parrod, J. J. Polym. Sci., Polym. Lett. Ed. 1963, 1, 329.
(8) Nguyen, A. B.; Hadjichristidis, N.; Fetters, L. J. Macromolecules 1986, 19, 768.
(9) Hild, G.; Kohler, E.; Rempp, P. Eur. Polym. J. 1980, 16, 525.
(10) Geiser, D.; Höcker, H. Macromolecules 1980, 13, 653.
(11) Roovers, J.; Toporowski, P. M. Macromolecules 1983, 16, 843.
(12) Kramers, H. A. J. Chem. Phys. 1946, 14, 415.
(13) Zimm, B.; Stockmayer, W. H. J. Chem. Phys. 1949, 17, 1301.
(14) Casassa, E. F. J. Polym. Sci., Part A 1965, 3, 605.
(15) Abramowitz, M.; Stegun, I. A. Handbook of Mathematical Functions; Dover: New York, 1970; p 319, Table 7.5.
(16) Burchard, W.; Schmidt, M. Polymer 1980, 21, 745.
(17) Akcasu, A. Z.; Gurol, H. J. Polym. Sci. 1976, 14, 1.
(18) Burchard, W. Macromolecules 1977, 10, 919.

Microstructure and Property Changes Accompanying Hard-Segment Crystallization in Block Copoly(ether–ester) Elastomers

Janis Castles Stevenson and Stuart L. Cooper*

Department of Chemical Engineering, University of Wisconsin—Madison, Madison, Wisconsin 53706. *Received August 25, 1987*

ABSTRACT: Hard-segment crystallization is a primary factor governing the properties of copoly(ether–ester) elastomers composed of poly(tetramethylene oxide) soft segments and poly(tetramethylene terephthalate) and/or poly(tetramethylene isophthalate) hard segments. Differential scanning calorimetry, tensile testing, and small-angle X-ray scattering have been used to follow the structure and property changes occurring during the room-temperature crystallization of copoly(ether–ester) elastomers in which poly(tetramethylene isophthalate) is the major hard-segment component. The measurements show that crystallization leads to significant improvements in tensile properties, particularly as the sample crystalline weight fraction increases from 0.05 to 0.10. These improvements have been attributed to hard-domain development from a dispersion of tie points that act as isolated entities to a network of cross-links that function collectively during deformation.

I. Introduction

Thermoplastic elastomers are materials that exhibit a unique combination of strength, flexibility, and processability due to their phase-separated microstructure. The elastomers are copolymers composed of two different types of segments, commonly referred to as "soft" and "hard" segments. The soft segments are derived from oligomers having a low glass transition temperature and are viscous at elastomer service temperatures, imparting flexibility to the material. Interactions between the hard segments lead to phase separation in which hard segment rich microdomains are formed that serve as physical cross links, contributing to the strength and dimensional stability of the material. Phase separation may involve hard segment vitrification, crystallization, hydrogen bonding, and/or ionic clustering.

One system in which hard-segment crystallization is particularly important is the copoly(ether–ester) elastomer based on soft segments of poly(tetramethylene oxide) (PTMO) and hard segments of poly(tetramethylene terephthalate) (PTMT) and/or poly(tetramethylene isophthalate) (PTMI) as illustrated in Figure 1. These copolymers have found extensive use in extrusion and molding resins for a wide variety of products. The morphology of such elastomers has been described in terms of a two-phase structure composed of crystalline hard domains relatively pure in hard segments and amorphous soft domains formed by a mixture of hard and soft segments.[1] The thermal and mechanical properties of the materials have been shown to vary with the fraction and type of hard-segment crystallinity present.[2] In order to understand such property variations, the underlying changes in polymer microstructure must be examined. In the present study, small-angle X-ray scattering measurements have been combined with differential scanning calorimetry and tensile measurements to elucidate the microstructure and property changes associated with hard-segment crystallization.

The crystallization rates of the copoly(ether–ester) elastomers depend upon which type of hard segment is the major crystallizing component. Copoly(ether–esters) in which PTMT is predominant crystallize rapidly upon cooling from the melt to room temperature; a substantial fraction of the crystallization occurs during cooling, even at cooling rates of 160 °C/min.[3] This leads to high production rates in manufacturing and is one reason why the commercial elastomers, marketed as Hytrel, contain primarily PTMT hard segments. However, the high crystallization rate makes it difficult to study the associated structure and property changes as they occur. In copoly(ether–esters) in which PTMI is the major hard-segment component, only a small amount of crystallization, if any, occurs during rapid cooling from the melt to room temperature. The samples are essentially transparent when removed from the mold, but, over a period of hours at room temperature, they gradually cloud with white specks and streaks and may eventually become entirely opaque. Simple probes such as flexing, stretching, or cutting the films at different degrees of opacity reveal remarkable changes in the properties of the copolymers. The crystallization rate is slow enough to allow these changes to be chronicled and quantified by using thermal, mechanical, and structural analysis techniques. On the basis of this characteristic, PTMI-rich copolyether–esters have been selected for this study of hard-segment crystallization.

II. Experimental Section

A. Materials. The copoly(ether–esters) used in this study were synthesized by melt transesterification of dimethyl terephthalate, dimethyl isophthalate, 1,4-butanediol, and poly(tetramethylene ether) glycol following a procedure similar to that described by Witsiepe.[4] A glycol with a number average molecular weight of approximately 1000 was used. Soft-segment crystallization is generally observed only for copolymers derived from glycols of 2000 MW or greater;[5,6] crystallization in the present materials was thus limited to the hard segments. The resultant segmented copolymers contain alternating soft-segment blocks

0024-9297/88/2221-1309$01.50/0

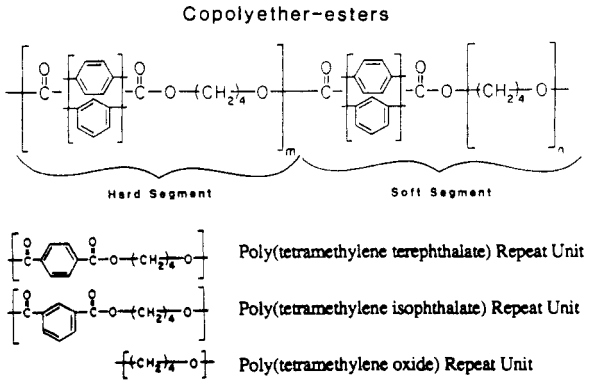

Figure 1. Copoly(ether–ester) chemical structure.

of PTMO and hard-segment blocks composed of random sequences of PTMI and/or PTMT as illustrated in Figure 1. The number average molecular weight of copolyether–esters so produced is typically 25 000–30 000. The two materials described in this paper each had a total hard-segment content of 60 wt % based on the conventional soft segment definition, which includes one isophthalate or terephthalate unit with each PTMO sequence as depicted in Figure 1. The hard-segment content is denoted by H60, and the hard-segment composition is designated by the two numbers that follow, which represent the PTMT:PTMI ratio. In the elastomer designated H60/0:100, the hard segments were only PTMI; in H60/10:90, the hard segments were composed of 10% PTMT and 90% PTMI. The materials were thermally stabilized with 0.2% *N,N'*-hexamethylenebis(3,5-di-*tert*-butyl-4-hydroxycinnamamide). The as polymerized samples were ground into powder form to ensure sample homogeneity. Grinding led to a rise of approximately four points in melt index and so may be responsible for some reduction in molecular weight.

B. Sample Preparation. Samples of the materials were prepared by compression molding the polymer powder between two Teflon-coated plates placed in a platen press at 25 °C above the as received polymer melting point and 104 MPa for 5 min. The press was cooled rapidly by circulating water through it until the temperature had dropped below 80 °C; the mold was then removed from the press and quenched with ice.

C. Differential Scanning Calorimetry. The thermal characteristics of the polymers were measured by using either a Perkin-Elmer DSC-2 or DSC-7. The calorimeters were calibrated for temperature and power by using indium and mercury melting as references. Helium was used to continuously purge the sample compartments. Samples of 7–15 mg were cut from the compression molded polymer films and sealed into Dupont aluminum pans. Thermal scans of the samples were collected during heating in the calorimeter at a rate of 20 °C/min. The glass transition temperatures of the copolymers were determined from the temperatures at which half of the total change in heat capacity had occurred. Crystalline fraction estimates were made from the enthalpies determined from the areas of the DSC melting endotherms. The base line of the endotherms did not correspond to a straight line in many instances, and therefore the Perkin-Elmer DSC software could not be used for area integration. Instead, a smooth curved base line that coincided with the DSC trace on either side of the endotherm(s) was used to define the area for integration. The crystalline fraction calculations were based on a heat of fusion of 192.1 J/(g of PTMI).[7]

D. Tensile Testing. Uniaxial stress–strain data were collected at room temperature with an Instron tensile tester using a crosshead speed of 1.27 cm/min. Dumbbell-shaped samples were cut from the compression molded films using an ASTM D-1708 die. The engineering stress data were calculated as the force divided by the initial cross-sectional area.

E. Small-Angle X-ray Scattering. X-rays were produced with an Elliott GX-21 rotating anode X-ray generator operated at an accelerating potential of 35 kV and an emission current of 15 mA. Following emission from the copper anode, the X-rays were passed through a nickel filter so that the X-ray wavelengths were predominantly 0.1542 nm (Cu Kα). A modified compact Kratky SAXS camera was used to collimate the X-rays into a beam that was approximately 1 cm by 100 μm at the sample. The

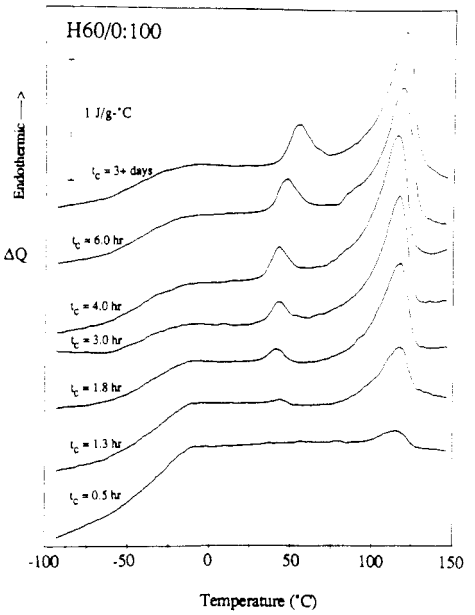

Figure 2. DSC traces for the heating at 20 °C/min of samples of H60/0:100 held at room temperature for various crystallization times, t_c.

collimation optics, the sample holder, and the scattering path were evacuated to eliminate scattering by air. The sample-to-detector distance was approximately 0.6 m. The detector was a TEC one-dimensional position-sensitive proportional counter containing a carbon-coated quartz anode. The scattering data were collected by a multichannel analyzer and transferred to a PDP 11/23 computer for subsequent processing.

Sets of scattering data were collected for periods of 10 min for H60/0:100 and 15 min for H60/10:90; the length of these periods was determined as a compromise between counting statistics and crystallization kinetics. One of the early scattering profiles for H60/0:100 had as few as 18 000 integrated counts from the scattering volume, but the counts were much greater for most of the profiles; for the samples of H60/10:90, the minimum number of integrated counts was 49 000. The data were smoothed prior to analysis; smoothing facilitated the determination of the background intensity but did not alter its value. Following smoothing, the data were corrected for detector sensitivity, dark current, parasitic scattering, and sample absorption. The scattering from a Lupolen polyethylene standard was used to restate the intensities on an absolute scale. An experimentally measured slit-length weighting function was used to desmear the data by the iterative method of Lake.[8]

III. Results and Discussion

A. H60/0:100 Crystallization. The transparency of compression molded films of H60/0:100 immediately following rapid cooling from the melt suggests that very little, if any, crystallization occurs during cooling. DSC measurements made within 30 min of the time at which the samples reach room-temperature feature a single glass transition and a small melting endotherm as illustrated in Figure 2. The midpoint of the glass transition occurs at approximately −34 °C. This represents a large elevation in glass transition temperature from that of pure PTMO, which has been reported as −84[9] to −88 °C,[10] and suggests that the uncrystallized hard segments are dispersed within the soft phase. Gordon and Taylor[11] proposed the following mixing rule for predicting the glass transition temperature of a copolymer

$$W_1(T_g - T_{g1}) + kW_2(T_g - T_{g2}) = 0 \qquad (1)$$

where W_1 and W_2 are the weight fractions of copolymer components 1 and 2, T_g is the glass transition temperature of the copolymer, T_{g1} and T_{g2} are the glass transition temperatures of the homopolymers of components 1 and

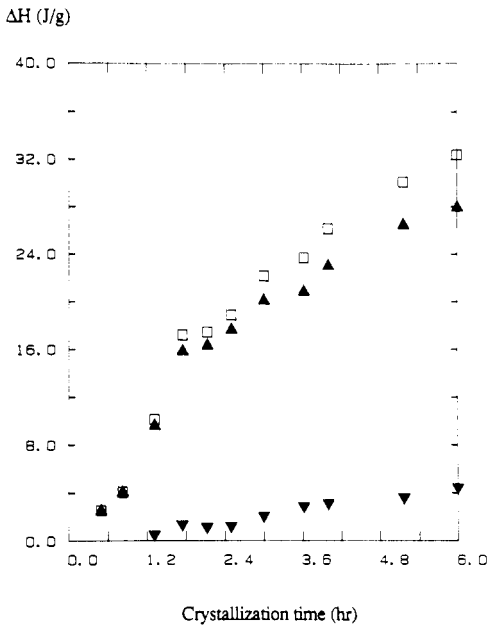

Figure 3. Enthalpy differences, ΔH, calculated from the areas of the DSC endotherms as a function of crystallization time at room temperature for samples of H60/0:100: (▼) annealing endotherm, (▲) melting endotherm, (□) sum of endotherms.

2, and k is given by the difference in thermal expansion coefficients between the rubbery and the glassy states of homopolymer 2 divided by that for homopolymer 1. In this case, let component 1 correspond to PTMO and component 2 be PTMI. If it is assumed that only the portion of the PTMI segments in the soft-phase contribute to the soft-phase glass transition temperature and that all of the uncrystallized PTMI segments are in the soft phase, W_1 and W_2 can be calculated. The crystalline weight fraction of the sample for t_c = 0.5 h is approximately 0.013 as determined from the area of the melting endotherm. The PTMI weight fraction of the sample is 0.678 (this is greater than the hard segment fraction because of the way in which the soft segment was defined) and W_2 = (0.678 − 0.013)/[(0.678 − 0.013) + 0.322] = 0.674, $W_1 = 1 - W_2$ = 0.326. For PTMO, let T_{g1} = −88 °C;[10] for PTMI, T_{g2} = 24 °C.[2] Experimental data for k is not readily available, but on the basis of the observed glass transition temperature of −34 °C, a value for k of 0.45 can be calculated. This is comparable with the value of 0.5 reported for k by Lilaonitkul and Cooper[12] for PTMT/PTMO copolymers based upon similar assumptions.

As crystallization proceeds, the area of the melting endotherm increases and the glass transition midpoint temperature decreases as the hard-segment content of the soft phase is reduced. After nearly an hour, an annealing endotherm is also detectable and increases in both temperature and area with time; the annealing endotherm has been attributed to an aggregation of initially uncrystallized hard segments into clusters whose ordering and/or size are temperature- and time-dependent and which represent additional phase separation.[2,13] The areas of the annealing and melting endotherms have been calculated and are shown as a function of time in Figure 3; although there is some uncertainty in determining the base line of the endotherms and the endotherms overlap, these calculations are useful as estimates of the enthalpies involved. The sample crystalline weight fraction associated with the melting endotherm is observed to increase from 0.013 at 0.5 h to a final value of 0.145, which is approached after approximately 6 h. Although it is not shown in Figure 3, the annealing endotherm continues to increase in area,

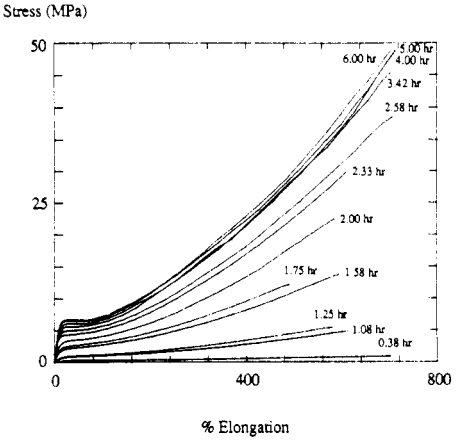

Figure 4. Stress as a function of percent elongation for samples of H60/0:100 crystallized at room temperature for various lengths of time.

from 4.4 J/g at 6 h to 5.2 J/g, which was measured after 3 days. As an indicator of the total amount of phase separation, the sum of the areas of the annealing and melting endotherms is also shown as a function of time in Figure 3.

Another indicator of the extent of phase separation is the soft-phase glass transition temperature. After 6 hours of crystallization, T_g has decreased to −42 °C. The crystalline weight fraction is approximately 0.145. The weight fraction of PTMI segments associated with the annealing-produced clusters is not known, but with the assumption that it is small relative to the crystalline weight fraction, W_2 can be approximated as (0.678 − 0.145)/[(0.678 − 0.145) + 0.322] = 0.623. With use of the value of k previously determined, T_g is predicted from eq 1 to be −40 °C. The phase separation associated with annealing would decrease the glass transition temperature further and would explain why the observed glass transition temperature is lower. To obtain T_g = −42 °C, W_2 must be 0.608, which would indicate that a fraction of 0.034 of the sample weight is involved in annealing clusters. After 3 days at room temperature, the glass transition temperature of the copolymer decreases to −44 °C while the crystalline weight fraction associated with the melting endotherm appears to remain constant, suggesting that the sample weight fraction involved in annealing clusters has increased to 0.048 assuming that eq 1 is valid.

Stress–strain measurements made during crystallization illustrate the dramatic changes that occur in the mechanical properties. Stress as a function of percent elongation is shown in Figure 4 for samples of H60/0:100 tested at various stages of crystallization. After approximately 0.4 h of crystallization, the crystalline weight fraction of the sample is approximately 0.01, and very little stress is required for elongation. As the crystalline fraction grows, the tensile curves show a pronounced increase in stress. Young's modulus and the yield stress have been calculated for each of the curves of Figure 4 and are plotted as a function of time in Figures 5 and 6, respectively. These two parameters appear to change in parallel manners: a moderate increase is observed during the first 1.25 h, a sharp increase is noted between 1.25 h and 2.6 h, and another period of moderate increase is detected from 2.6 h to 6.0 h. Cella[14] suggested that Young's modulus is a measure of the force required to pseudoelastically deform the crystalline cross-link network in the copolymer and that the yield stress is a measure of the force required to orient the crystallites in the draw direction. At early stages of crystallization, the cross-links are sparse and their effects

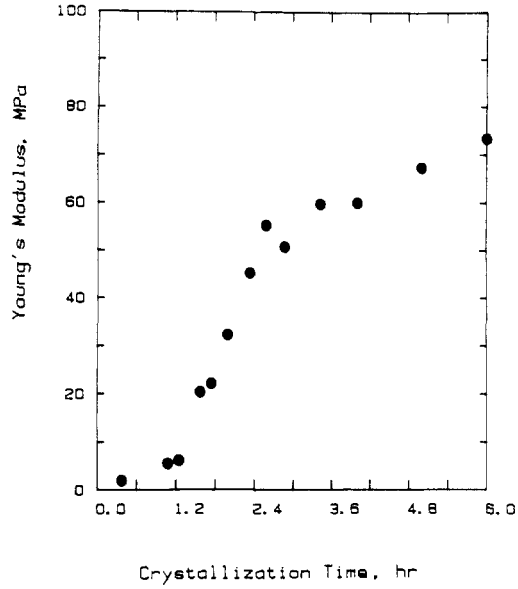

Figure 5. Young's modulus as a function of crystallization time at room temperature for samples of H60/0:100.

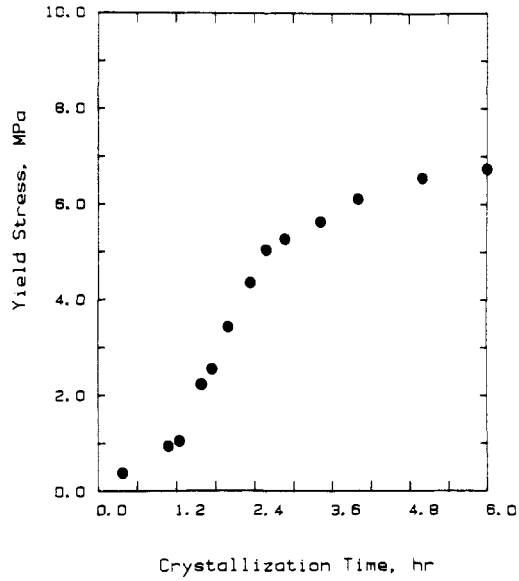

Figure 6. Yield stress as a function of crystallization time at room temperature for samples of H60/0:100.

are mostly localized, so that little stress is required to deform the polymer. As the crystalline fraction increases, the extent of cross-linking increases, and Young's modulus and the yield stress are observed to rise. After 1.25 h, the crystalline weight fraction of the sample is approximately 0.05; this marks the onset of a steep increase in Young's modulus and yield stress that extends to a time of 2.6 h and a crystalline fraction of approximately 0.10. It is proposed that, during this period, the structure evolves from a dispersion of isolated cross-links to an interconnected network of crystalline tie points; an analogy of this transformation could be drawn with gelation in chemically cross-linked polymers. Crystallization beyond a sample weight fraction of 0.10 increases Young's modulus and the yield stress due to additional cross-links, but the effect is not as great.

Small angle X-ray scattering has been used to monitor changes in the microstructure. The scattering profiles for various crystallization times are shown in Figure 7. The scattered intensities, $I(q)$, have been normalized by the intensity scattered by a single electron, $I_e(q)$, and the scattering volume, V, and are plotted as a function of the

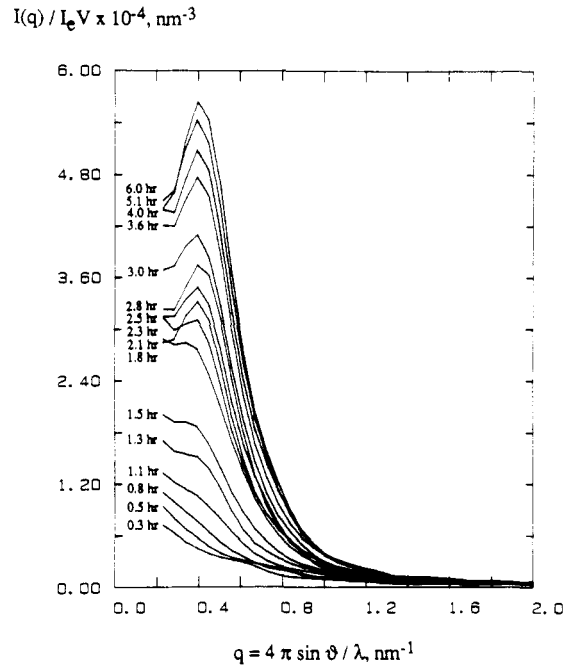

Figure 7. Small-angle X-ray scattering profiles during room temperature crystallization of a sample of H60/0:100.

scattering vector magnitude, q; q is related to the angle at which the X-rays are scattered by

$$q = 4\pi \sin \theta/\lambda \quad (2)$$

where θ is half the scattering angle and λ is the radiation wavelength. The intensity data are shown for $q = 0.2$ nm^{-1} to $q = 2.0$ nm^{-1} in order to highlight the peak region; the data actually extend up to $q = 5.8$ nm^{-1} but show only a gradual decrease to a constant limiting value. The data have been truncated at $q = 0.2$ nm^{-1} due to intensity contributions at lower q caused by scattering from the instrument beam stop.

In the early stages of crystallization, the scattering profiles exhibit a gradual decrease in intensity with increasing q. As time increases, the intensities grow and a well-defined scattering peak emerges at approximately 1.3 h. The peak shifts to higher values of q as the time increases to 2.3 h. After 2.3 h, the peak continues to increase in magnitude but remains at the same position in q. This profile development is qualitatively similar to that described by Vignaud and Schultz[15] in a simulation of the development of SAXS profiles for a classical nucleation and growth model of polymer crystallization. In this model, nucleation is assumed to be heterogeneous and to take place at time zero. Crystallites grow from the nucleating sites to form lamellar stacks of alternating amorphous and crystalline phases. The intercrystalline distances are distributed in a paracrystalline manner. Crystallite growth occurs both by stack extension and by lamellar thickening. The thickening rate is assumed to have a logarithmic dependence on time. The qualitative similarity of the simulated profile development to that of the present data suggests that this model may hold promise for quantitative simulation of the data. Before such a simulation is attempted, however, a better understanding of the basic crystallization process in this system is desirable.

From the scattering data, the long period, L, an estimate of the magnitude of the domain spacing, can be determined

$$L = 2\pi/q_{peak} \quad (3)$$

where q_{peak} is determined from the maximum of a plot of

$q^2I(q)$ versus q. Once the scattering peak position attains a constant value of q, the long period is calculated to be 12.3 nm. This is comparable with the long spacing observed in copoly(ether–esters) in which PTMT is the major crystallizing component.[16,17]

The intensity data in the tail region of the scattering curve can be related to the magnitude of the scattering vector using a power law expression. Porod[18–20] showed that the small-angle scattering from a dilute isotropic collection of scattering particles approaches a limiting value in the tail of the scattering curve according to

$$\lim_{q\to\infty} q^4I(q) = K \tag{4}$$

where K is known as Porod's constant. This equation is valid for any shape of particle provided that the orientations of the particles are random and that $qD \gg 1$ for every dimension D of the particles. Although the relationship was originally derived for a dilute collection of particles, it has also been found to hold for many densely packed systems and nonparticulate structures as well. For two-phase systems in which the boundaries between the phases are not sharply defined and the electron densities of the phases are not entirely homogeneous, Ruland[21] suggested a modification to this relationship

$$I(q) = I_p(q)H^2(q) + I_b(q) \tag{5}$$

where $I_p(q)$ is the intensity predicted by Porod's law (eq 4), $H^2(q)$ is an expression representing the effects of a diffuse interface, and $I_b(q)$ embodies scattering contributions due to thermal density fluctuations, phase mixing, and the onset of wide angle X-ray diffraction. $H^2(q)$ is given by the Fourier transform of the self-convolution of the electron density gradient describing the interface.

A nonlinear regression computer program was used to fit eq 5 normalized by the intensity scattered by a single electron, I_e, and the scattering volume, V, to the scattering data. The background intensity was fitted in the range of $3.0 \le q \le 5.8$ nm^{-1} and was described satisfactorily by a single constant, A. The interface was represented by a function of the form

$$H^2(q) = (\sqrt{3}\sigma q)^2 \operatorname{cosech}^2(\sqrt{3}\sigma q) \tag{6}$$

This expression corresponds to a Cahn–Hilliard-type density profile for a block copolymer at equilibrium conditions[22–24]

$$\rho(x) = [(\rho_2 - \rho_1)/2] \tanh(\pi x/\sigma\sqrt{12}) + [(\rho_2 + \rho_1)/2] \tag{7}$$

where x is the distance from the center line of the interfacial region, ρ_1 is the density of phase 1, ρ_2 is the density of phase 2, and σ is a parameter characterizing the width of the interfacial region. Poor fits were obtained for data collected at crystallization times less than 2.6 h; the intensity data did not conform to a fourth power dependence on q, so the exponent of q, which will be referred to as m, was allowed to vary. Adjustment of K and m permitted good fits to be obtained for every profile over the range of $0.6 \le q \le 5.8$ nm^{-1}. Variation of the fitting range had only small effects on the values of the parameters. The values of K, m, and A yielding the best fits to the $I(q)/I_e(q)V$ data with $\sigma = 0$ are listed in Table I. K rises for the first 4 h and then begins to level off. The exponent, m, begins at a value of approximately 2.4 and increases to a value of 4.0 in 2.5 h, after which it remains constant. The background constant, A, fluctuates but does not reveal any clear time dependence. Inclusion of the interfacial thickness parameter, σ, in the regression only improved the fits of the profiles corresponding to the first hour of crystallization. Even then, σ amounted to 0.3 nm or less, suggesting that the boundaries between the phases are relatively sharp. Inclusion of σ elevated K by approximately 10% for the early profiles and lowered m, decreasing it to 2.1 at 0.25 h.

Table I
Scattering Parameters Determined by Fitting $I(q)/I_e(q)V = K/q^m + A$ to Small-Angle X-ray Scattering Data for H60/0:100

crystallizatn time, h	$K \pm 2$ std dev, nm^{m-3}	$m \pm 2$ std dev, unitless	$A \pm 2$ std dev, nm^{-3}
0.25	794 ± 27	2.47 ± 0.09	116 ± 9
0.50	1008 ± 28	2.41 ± 0.07	155 ± 10
0.75	966 ± 36	2.64 ± 0.10	151 ± 11
1.05	1222 ± 30	2.90 ± 0.07	125 ± 8
1.25	1503 ± 36	3.09 ± 0.07	116 ± 10
1.50	1695 ± 45	3.44 ± 0.08	133 ± 9
1.78	2385 ± 50	3.54 ± 0.06	140 ± 8
2.05	2421 ± 53	3.66 ± 0.07	130 ± 7
2.30	2515 ± 49	3.74 ± 0.06	127 ± 8
2.53	2700 ± 60	3.79 ± 0.07	134 ± 10
2.77	2631 ± 52	3.97 ± 0.06	146 ± 9
3.00	2903 ± 57	4.00 ± 0.06	142 ± 7
3.55	3399 ± 80	4.01 ± 0.07	159 ± 8
4.02	3748 ± 82	4.02 ± 0.07	167 ± 10
5.10	3905 ± 74	3.95 ± 0.06	167 ± 9
6.00	3894 ± 95	4.04 ± 0.08	209 ± 11

Some physical justification for the variation in m is necessary to interpret this data. It was mentioned earlier that Porod's law is based on two assumptions: the scattering particles are randomly oriented and $qD \gg 1$ for every dimension D of the scattering particles. While it is likely, based upon the preparation method, that the first assumption is valid for this system, it is quite possible that the second requirement is not satisfied at early stages of crystallization. For example, if $q = 0.6$ nm^{-1}, D must be significantly greater than 1.7 nm; this may not hold for every dimension of the crystalline embryos. Even when the lower q limit of the fitting range is increased, m does not appear to approach 4 for the early profiles, suggesting that at least one dimension of the embryos is quite small. It has been shown (e.g., refer to Glatter and Kratky[25] or Guinier et al.[26]) that for flat, disklike particles in which the disk radius satisfies $qD \gg 1$ but the disk thickness does not, m approaches 2 as q goes to infinity. One might speculate, based on the initial value of m which is close to 2 for H60/0:100, that the crystalline PTMI embryos are only angstroms thick in one dimension. This dimension increases with time such that $qD \gg 1$ is satisfied after 2.5 h and m approaches 4. One possibility is that the thin dimension corresponds to the lamellar thickness. Martinez-Salazar, Barham, and Keller[27] have described polyethylene crystallization from the melt in terms of a process involving the formation of relatively thin lamellae that thicken isothermally, first in a single large step and then logarithmically with time. The model of Vignaud and Schultz[15] described previously also involves lamellar thickening. If such a mechanism should hold true for the melt crystallization of the much shorter sequences found in block copolyether–esters, the variation in m might suggest that the initial lamellae are only one or two PTMI repeat units thick. Line-broadening information from wide-angle X-ray diffraction experiments might support this speculation; these experiments have not been performed to date because the quality of the data obtained at such low crystallinities is generally poor. Although the diffraction pattern of PTMI crystallinity is known,[2] it has not been indexed; the indexing would allow one to identify which crystal dimensions are particularly small.

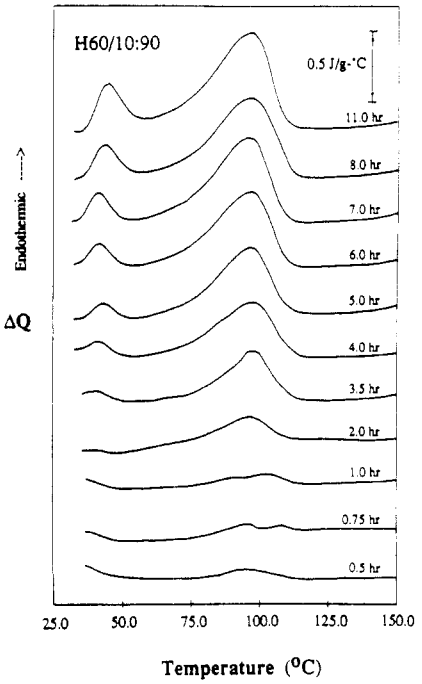

Figure 8. DSC traces for the heating at 20 °C/min of samples of H60/10:90 held at room temperature for various crystallization times, t_c.

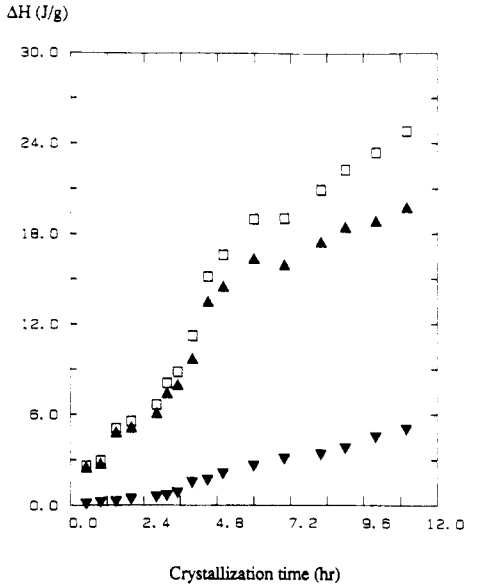

Figure 9. Enthalpy differences, ΔH, calculated from the areas of the DSC endotherms as a function of crystallization time at room temperature for samples of H60/10:90: (▼) annealing endotherm, (▲) melting endotherm, (□) sum of endotherms.

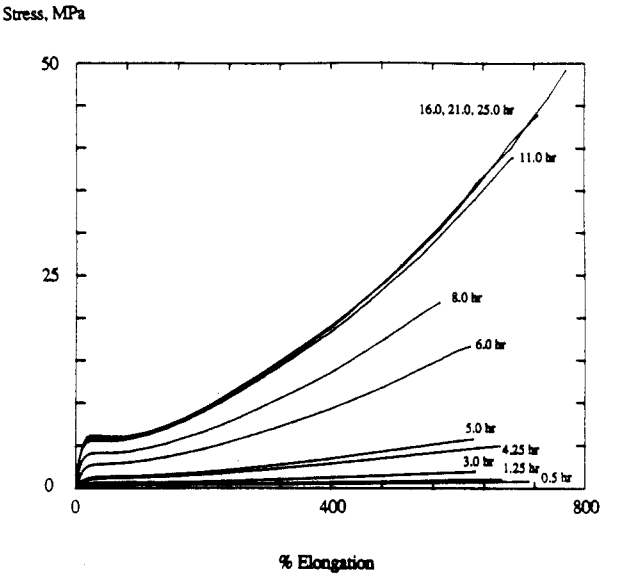

Figure 10. Stress as a function of percent elongation for samples of H60/10:90 crystallized at room temperature for various lengths of time.

In examining the thermal, tensile, and scattering data together, it is interesting to note that the onset of the sharp increase in Young's modulus and yield stress shown in Figures 5 and 6 appears to coincide in time with the emergence of the scattering peak shown in Figure 7. The crystalline weight fraction of the sample at this point as measured from the melting endotherm is approximately 0.05 and m is about 3. The end of the sharp rise in Young's modulus and yield stress occurs at approximately the same time that the crystalline fraction nears 0.10, the scattering peak position becomes fixed, and m reaches 4. The significance of these observations will be addressed following an examination of the crystallization data for H60/10:90.

B. H60/10:90 Crystallization. When the hard segments contain 10% PTMT, the PTMI crystallization rate at room temperature is significantly decreased. A compilation of DSC scans for H60/10:90 samples crystallized for various lengths of time is shown in Figure 8. The presence of one endotherm at 0.5 h and two distinguishable endotherms at 0.75 and 1.0 h suggests that the initial endotherm is associated with crystals originated during cooling from the melt. The initial crystalline fraction appears to be on the order of 0.01 of the sample weight. The remaining crystallization occurs at room temperature and is nearly completed after approximately 12 h, although the annealing endotherm continues to increase beyond this time. The enthalpies associated with the annealing and melting endotherms are shown as a function of time in Figure 9. The slight dip in melting endotherm enthalpies that appears between 6 and 8 h is due to uncertainties in determining the endotherm area; it does not reflect any decrease in crystalline fraction.

The soft-phase glass transition midpoint temperature of the polymer is observed to decrease gradually over this 12-h period from approximately −33 to −43 °C. The enthalpy associated with the melting endotherm after 11 h of crystallization amounts to 19.7 J/g or a sample weight fraction of 0.102 and that of the annealing endotherm totals 5.1 J/g. On the basis of these estimates, the fraction of hard segments in the soft phase should be greater than for H60/0:100 and one might expect the glass transition temperature to be higher than −43 °C; however, the relationship used to predict T_g for H60/0:100 may not be applicable for H60/10:90, particularly in light of the introduction of a third component, PTMT.

The stress–strain properties measured during crystallization are illustrated as a function of time in Figure 10. A large change is noted in the curves between 4.25 and 11.0 h; the difference between the curves for 5.0 and 6.0 h is particularly striking. Young's modulus and the yield stress have been determined for each of the curves and are shown in Figures 11 and 12. These parameters show only a slight increase for the first 3.0 h. The increase picks up after 3.0 h and then rises sharply between about 4.25 and 10.0–11.0 h. Only a slight increase is noted past 11.0 h. The crystalline weight fraction at the onset of the sharp increase is approximately 0.05 and at the end of the sharp rise is 0.10. This is similar to what was observed for H60/0:100.

The small-angle X-ray scattering profiles for H60/10:90 are presented in Figure 13. The scattered intensity decreases with increasing q for the profiles collected for

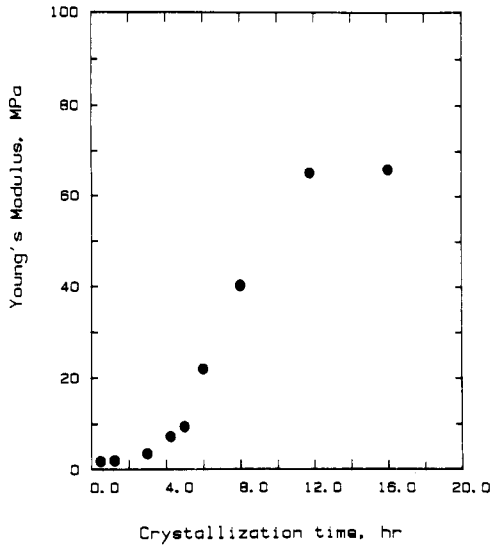

Figure 11. Young's modulus as a function of crystallization time at room temperature for samples of H60/10:90.

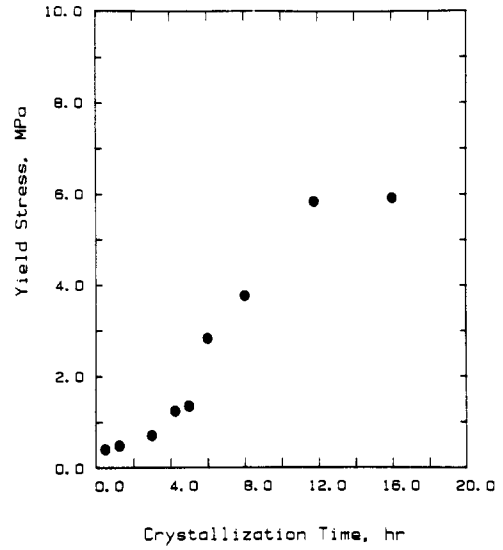

Figure 12. Yield stress as a function of crystallization time at room temperature for samples of H60/10:90.

crystallization times of less than approximately 4 h. By 4.9 h, a scattering peak has emerged. The peak increases greatly in magnitude with time but changes little in q; the long period corresponds to approximately 12.7 nm. A similar approach to that described for the analysis of the scattering data for H60/0:100 was used. A constant was used to fit the background intensity in the range of $3.0 \leq q \leq 5.8$ nm^{-1}. Parameters K, σ, and m were fitted in the range of $0.6 \leq q \leq 5.8$ nm^{-1}. The values of K, m, and A producing the best fits when σ is fixed at zero are listed in Table II. K is relatively constant for the first 3 h and rises gradually up to about 11 h. The value of m is about 2.6 at 0.5 h and approaches 4.0 near the end of the crystallization period. The background constant, A, tends to decrease. Allowing σ to vary during regression improves the fits significantly for profiles collected during the first 4 h of crystallization, although σ is relatively small, never more than 0.42 nm. In these early profiles, it raises the value of K by about 20% and lowers the initial value of m to approximately 1.8. On the basis of the interpretation suggested earlier for the variation of m, it would appear that the final crystallite sizes attained in H60/10:90 are smaller in at least one dimension than those of H60/0:100 since m approaches 4 (i.e., $qD \gg 1$ is approached) only near the very end of the crystallization period.

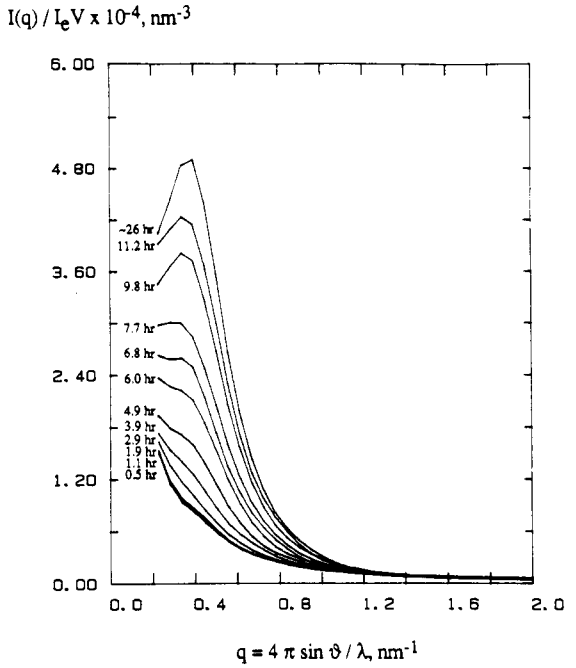

Figure 13. Small-angle X-ray scattering profiles during room-temperature crystallization of a sample of H60/10:90.

Table II
Scattering Parameters Determined by Fitting $I(q)/I_e(q)V = K/q^m + A$ to Small-Angle X-ray Scattering Data for H60/10:90

crystallizatn time, h	$K \pm 2$ std dev, nm^{m-3}	$m \pm 2$ std dev, unitless	$A \pm 2$ std dev, nm^{-3}
0.53	1241 ± 30	2.55 ± 0.05	264 ± 4
1.07	1238 ± 31	2.55 ± 0.05	247 ± 4
1.92	1202 ± 29	2.63 ± 0.05	245 ± 5
2.92	1268 ± 30	2.76 ± 0.05	225 ± 4
3.88	1387 ± 27	2.90 ± 0.05	220 ± 4
4.85	1535 ± 29	3.06 ± 0.05	214 ± 3
5.97	1826 ± 34	3.22 ± 0.05	202 ± 4
6.83	1944 ± 34	3.44 ± 0.05	213 ± 3
7.65	2162 ± 36	3.51 ± 0.04	201 ± 3
9.75	2624 ± 48	3.59 ± 0.05	179 ± 4
11.18	2693 ± 46	3.78 ± 0.05	181 ± 4
~26	2914 ± 53	3.87 ± 0.05	149 ± 4

C. Structure and Property Development during Crystallization. On the basis of the observations of structure and property changes during room-temperature crystallization of H60/0:100 and H60/10:90, the following mechanism is proposed. As the copolymer is cooled from the melt to room temperature, nucleation and a small amount of PTMI crystallite growth may occur. The crystalline embryos are small, perhaps only angstroms thick in one dimension, and are relatively isolated from one another. The difference in electron densities between the crystalline embryos and the soft phase gives rise to small-angle X-ray scattering, but there is not sufficient periodicity to produce a scattering peak. The tensile strength of the polymer is slightly improved as a few crystalline ties develop, but the effects are mostly localized and little stress is required to elongate the sample. PTMI crystallization proceeds at room temperature, requiring at least 6 h for H60/0:100 and at least 12 h for H60/10:90. Crystallization reduces the fraction of hard segments in the soft phase and leads to a decrease in glass transition temperature and an increase in scattering. As the crystalline weight fraction of the sample nears 0.05, the periodicity of the electron density variation becomes defined and a scattering peak becomes detectable. With further

crystallization, the scattering peak grows in magnitude but the long period remains essentially constant except for a slight decrease that may be observed immediately following the initial appearance of the peak. Once the PTMI segments of individual chains start to become tied into more than one crystalline lamella, the tensile strength of the polymer begins to improve significantly. The polymer structure evolves from a system in which the hard domains act as isolated tie points to a system in which the hard domains function as an interconnected network. Deformation is transformed from a local to a global process, in which a tug on one chain exerts a force on a large number of other chains to which it is tied either directly or indirectly. A network of hard domain ties of at least skeletal proportion is achieved by the time the crystalline weight fraction has reached approximately 0.10. Further crystallization provides additional cross-linking that enhances the tensile properties, but the incremental changes are not as large.

IV. Summary

The hard-segment crystallization of two copoly(ether–ester) elastomers in which PTMI is the crystallizing component has been studied at room temperature by using differential scanning calorimetry, stress–strain, and small-angle X-ray scattering measurements. When the samples are prepared by rapid cooling from the melt to room temperature, crystallization requires a minimum of 6 h for H60/0:100 and at least 12 h for H60/10:90. The DSC scans feature a soft phase glass transition, an annealing endotherm, and a melting endotherm. The glass transition midpoint temperature decreases as the areas of the annealing and melting endotherms increase and is evidence of the increase in phase separation between the hard and soft segments that occurs during crystallization and annealing. A scattering peak develops in the SAXS profiles once a crystalline fraction of approximately 0.05 of the sample weight is attained. The scattering peak may initially shift to slightly higher values of the scattering vector magnitude, q, but then remains essentially fixed in q while it exhibits large increases in size. This scattering profile development is qualitatively similar to that simulated by Vignaud and Schultz[15] for a classical nucleation and growth model of polymer crystallization. Crystallization leads to significant improvements in tensile properties, particularly as the sample crystalline weight fraction increases from 0.05 to 0.10. These improvements have been attributed to an evolution in structure during hard-segment crystallization from a dispersion of tie points that act as isolated entities to a network of cross-links that function collectively during deformation.

Acknowledgment. We wish to thank Dr. J. Michael McKenna, Polymer Products Department, E. I. duPont de Nemours & Co., for the synthesis of our copolymers. We wish to acknowledge partial support of this work by the Division of Materials Research, National Science Foundation, through Grant No. DMR-86-03839. J.C.S. would also like to thank the National Science Foundation for support through a graduate fellowship and research assistantships.

Registry No. H60/0:100, 113451-46-0; H60/10:90, 107811-95-0.

References and Notes

(1) Buck, W. H.; Cella, R. J., Jr. *Polym. Prepr. (Am. Chem. Soc., Div. Polym. Chem.)* **1973**, *14*, 98.
(2) Castles, J. L.; Vallance, M. A.; McKenna, J. M.; Cooper, S. L. *J. Polym. Sci., Polym. Phys. Ed.* **1985**, *23*, 2119.
(3) Stevenson, J. C.; Cooper, S. L. *J. Polym. Sci., Polym. Phys. Ed.*, in press.
(4) Witsiepe, W. K. *Adv. Chem. Ser.* **1973**, *129*, 39.
(5) Ghaffar, A.; Goodman, I.; Hall, I. H. *Br. Polym. J.* **1973**, *5*, 315.
(6) Boussias, C. M.; Peters, R. H.; Still, R. H. *J. Appl. Polym. Sci.* **1980**, *25*, 855.
(7) Conix, A.; van Kerpel, R. *J. Polym. Sci.* **1959**, *40*, 521.
(8) Lake, J. A. *Acta Crystallogr.* **1967**, *23*, 191.
(9) Wetton, R. E.; Allen, G. *Polymer* **1966**, *7*, 331.
(10) Yoshida, S.; Suga, H.; Seki, S. *Polym. J.* **1973**, *5*, 25.
(11) Gordon, M.; Taylor, J. S. *J. Appl. Chem.* **1952**, *2*, 493.
(12) Lilaonitkul, A.; West, J. C.; Cooper, S. L. *J. Macromol. Sci., Phys.* **1976**, *B12*, 563.
(13) Stevenson, J. C. Ph.D. Thesis, University of Wisconsin, 1987.
(14) Cella, R. J. *J. Polym. Sci., Polym. Symp.* **1973**, *C42*, 727.
(15) Vignaud, R.; Schultz, J. M. *Polymer* **1986**, *27*, 651.
(16) Bandara, U.; Dröscher, M. *Colloid Polym. Sci.* **1983**, *261*, 26.
(17) Perego, G.; Cesari, M.; Vitali, R. *J. Appl. Polym. Sci.* **1984**, *29*, 1157.
(18) Porod, G. *Kolloid-Z.* **1951**, *124*, 83.
(19) Porod, G. *Kolloid-Z.* **1952**, *125*, 51.
(20) Porod, G. *Kolloid-Z.* **1952**, *125*, 108.
(21) Ruland, W. *J. Appl. Crystallogr.* **1971**, *4*, 70.
(22) Cahn, J. W.; Hilliard, J. E. *J. Chem. Phys.* **1958**, *28*, 258.
(23) Helfand, E. *Acc. Chem. Res.* **1975**, *8*, 295.
(24) Roe, R. J.; Fishkis, M.; Chang, J. C. *Macromolecules* **1981**, *14*, 1091.
(25) *Small Angle X-Ray Scattering*; Glatter, O., Kratky, O., Eds.; Academic: New York, 1982.
(26) Guinier, A.; Fournet, G.; Walker, C. B.; Yudowitch, K. L. *Small Angle Scattering of X-Rays*; Wiley: New York, 1955.
(27) Martinez-Salazar, J.; Barham, P. J.; Keller, A. *J. Mater. Sci.* **1985**, *20*, 1616.